Articles

Competitive Surface Adsorption of Solvent Molecules and Compactness of Agglomeration in Calcium Hydroxide Nanoparticles

Emiliano Fratini,[†] Miles G. Page,*[,‡] Rodorico Giorgi,[†] Helmut Cölfen,[‡] Piero Baglioni,[†] Bruno Demé,[§] and Thomas Zemb[||]

Department of Chemistry and CSGI, University of Florence, via della Lastruccia 3, 50019 Sesto Fiorentino, Florence, Italy, Max Planck Institute for Colloids and Interfaces, Am Mühlenberg 1, Golm 14476 Germany, Institut Laue−Langevin, 6 rue Jules Horowitz, BP 156, F-38042 Grenoble Cedex 9, France, and Service de Chimie Moléculaire, bat. 125, 91191 Gif sur Yvette Cedex, France

Received July 12, 2006. In Final Form: November 6, 2006

Calcium hydroxide forms unstable reactive nanoparticles that are stabilized when they are dispersed in ethylene glycol or 2-propanol. The aggregation behavior of these particles was investigated by contrast-variation small-angle neutron scattering (SANS), combined with small-angle X-ray scattering (SAXS). Nanoparticles on the order of 100 nm were found to aggregate into mass-fractal superstructures in 2-propanol, while forming more compact agglomerated aggregates with surface fractal behavior in ethylene glycol. Commensurate specific surface areas evaluated at the Porod limit were more than an order of magnitude greater in 2-propanol ($\sim$200 $m^2 \cdot g^{-1}$) than in ethylene glycol ($\sim$7 $m^2 \cdot g^{-1}$). This profound microstructural evolution, observed in similar solvents, is shown to arise from competitive solvent adsorption. The composition of the first solvent layer on the particles is determined over the full range of mixed solvent compositions and is shown to follow a quantifiable thermodynamic equilibrium, determined via contrast-variation SANS, that favors ethylene glycol over 2-propanol in the surface layer by about 1.4 $kJ \cdot mol^{-1}$ with respect to the bulk solvent composition.

Introduction

Several examples of dispersions of precipitated inorganic particles that display unusual material properties have recently been reported. Most significantly, both Rieger et al.[1,2] and Ballauff and co-workers[3,4] have observed the precipitation of crystalline calcium carbonate through amorphous precursor nanoparticles. These can be stabilized by additives such as a polycarboxylate, which fixes the nascent particles in a polymer−Ca^{2+} microgel network. Furthermore, biomineralization and biomimetic mineralization using particle-associating polymers to direct crystal growth has been shown[5−8] to follow a similar mechanism of precursor nanocrystal stabilization via polymer adsorption and the generation of amorphous precursor phases prior to crystallization.

The identification and characterization of such transient particles represents a significant challenge, in an emerging field where such particles can also be building blocks for single crystals[9] and where fundamental study of ionic precipitation is reintroduced as an essential tool in nanoparticle synthesis and the study of biological mineralization. Nanocrystals as building units of a final single crystal have so far mainly been observed in presence of polymeric stabilizers, with the exceptions of DL-alanine,[10] cobalt oxalate dehydrate,[11] iron[12] and cobalt[13] oxyhydroxides, and silver nanoparticles,[14] as crystallographically aligned nanoparticle subunits usually fuse to form a single crystal before they can be observed. It is therefore of great interest to observe such single-crystal nanoparticles in calcium systems without polymeric stabilizers, before and during their controlled self-organization.[15,16]

Dei, Baglioni, and co-workers[17−21] have synthesized several examples of calcium hydroxide nanoparticles with controllable stability, a crucial property for applications. In particular, calcium (and magnesium) hydroxide nanoparticles applied in consolidation of wall painting and for paper and wood deacidification[18,22,23]

* Corresponding author: e-mail miles.page@mpikg.mpg.de.
[†] University of Florence.
[‡] Max Planck Institute for Colloids and Interfaces.
[§] Institut Laue−Langevin.
[||] Service de Chimie Moléculaire.

(1) Rieger, J.; Thieme, J.; Schmidt, C. *Langmuir* **2000**, *16*, 8300.
(2) Rieger, J. *Tenside, Surfactants, Deterg.* **2002**, *39*, 221.
(3) Pontoni, D.; Bolze, J.; Dingenouts, N.; Narayanan, T.; Ballauff, M. *J. Phys. Chem. B* **2003**, *107*, 5123.
(4) Bolze, J.; Peng, B.; Dingenouts, N.; Panine, P.; Narayanan, T.; Ballauff, M. *Langmuir* **2002**, *18*, 8364.
(5) Politi, Y.; Arad, T.; Klein, E.; Weiner, S.; Addadi, L. *Science* **2004**, *306*, 1161.
(6) Weiner, S.; Sagi, I.; Addadi, L. *Science* **2005**, *309*, 1027.
(7) Yu, S. H.; Cölfen, H. *J. Mater. Chem.* **2004**, *14*, 2124.
(8) Cölfen, H.; Mann, S. *Angew. Chem., Int. Ed.* **2003**, *42*, 2350.
(9) Cölfen, H.; Antonietti, M. *Angew. Chem., Int. Ed.* **2005**, *44*, 5576.
(10) Ma, Y.; Cölfen, H.; Antonietti, M. *J. Phys. Chem. B* **2006**, *110*, 10822
(11) Pujol, O.; Bowen, P.; Stadelmann, P. A.; Hofmann, H. *J. Phys. Chem. B* **2004**, *108*, 13128.
(12) Banfield, J. F.; Welch, S. A.; Zhang, H. Z.; Ebert, T. T.; Penn, R. L. *Science* **2000**, *289*, 751.
(13) Penn, R. L.; Stone, A. T.; Veblen, D. R. *J. Phys. Chem. B* **2001**, *105*, 4690.
(14) Van Hyning, D. L.; Klemperer, W. G.; Zukoski, C. F. *Langmuir* **2001**, *17*, 3128.
(15) Ocana, M.; Rodriguezclemente, R.; Serna, C. J. *Adv. Mater.* **1995**, *7*, 212.
(16) Adair, J. H.; Suvaci, E. *Curr. Opin. Colloid Interface Sci.* **2000**, *5*, 160.
(17) Nanni, A.; Dei, L. G. *Langmuir* **2003**, *19*, 933.
(18) Giorgi, R.; Dei, L.; Ceccato, M.; Schettino, C.; Baglioni, P. *Langmuir* **2002**, *18*, 8198.
(19) Salvadori, B.; Dei, L. *Langmuir* **2001**, *17*, 2371.
(20) Ambrosi, M.; Dei, L.; Giorgi, R.; Neto, C.; Baglioni, P. *Langmuir* **2001**, *17*, 4251.
(21) Ambrosi, M.; Dei, L.; Giorgi, R.; Neto, C.; Baglioni, P. *Prog. Colloid Polym. Sci.* **2001**.

10.1021/la062023i CCC: $37.00
Published on Web 02/02/2007

have provided clear evidence of the huge potential of nanotechnology in cultural heritage conservation,[24,25] and the same nanosized hydroxides were successfully used for consolidation of the recently discovered "Maya" paintings.[26]

Recently, surfactant-free calcium hydroxide nanoparticle agglomerates were synthesized[19] at high temperature in 1,2-propanediol or 1,2-ethanediol (ethylene glycol, EG). These particles aggregate strongly in EG (or water) to form ~micrometer-sized agglomerates. They can, however, be "peptized" (deaggregated) by washing with, for example, 2-propanol (2P) to yield individual nanoparticle units. This deaggregating effect was proposed to have resulted from physisorption of 2P molecules to the particle surface, and the hexagonal platelets of crystalline calcium hydroxide were proposed to have formed aligned particle stacks, on the basis of wide-angle X-ray scattering data that showed increased relative intensity of the basal (001) crystallographic face.[19] Adsorption of solvent molecules onto surfaces of mineral nanoparticles leading to their subsequent stabilization was also recently observed in the synthesis of stable nanoparticle dispersions in benzyl alcohol.[27]

The aim of this study is to investigate the role of ethylene glycol and 2-propanol adsorption in the stabilization as well as compactness of agglomeration of calcium hydroxide nanoparticles. Characterization is performed in situ by small-angle X-ray scattering (SAXS) and small-angle neutron scattering (SANS) with contrast variation in 2P and EG solvents, as well as in mixtures of the two. In the absence of a strong solubilizer like water, aging of the particles is effectively frozen, allowing direct examination of stabilization effects by the two solvents, in what would otherwise be the early stages of crystal growth by nanocrystal aggregation that can be considered analogous to the effect of the polymeric stabilizers described above, in a simple, additive-free system.

In the absence of specific adsorption, and with particle morphology independent of deuteration, absolute-scaled small-angle scattering alone would be sufficient to determine both the solvent content "inside" an agglomerated particle and the total surface area per unit volume of sample.[28] However, it has been shown that contrast variation in SANS can be used to determine the composition of a layer adsorbed on any colloidal structure.[29−31] The key point is that the contrast-match point (CMP) versus density of deuterium nuclei in the solvent gives direct information about the average scattering-length density of the "particle". If solvent is adsorbed to the particle and if the composition of bound solvent is different from bulk, then the particle appears as if swollen by the adsorbed solvent.

Moreover, the standard plot giving the square root of scattering at zero angle versus deuterium content is nonlinear in the case of preferential adsorption. The contrast-variation method has been extended to nonzero angles,[32] and this general method, unique to determine specific adsorption by components in mixed solvents,[33,34] is used here to investigate peptization of nanoparticles.

Table 1. SANS Sample Data for $Ca(OH)_2$ Nanoparticles in Various Solvents

χ^a	σ_{solv}, g cm^{-3}	$10^6 \times$ SLD$_{part}$,[b] Å^{-2}	$10^6 \times$ SLD$_{solv}$,[c] Å^{-2}	$Ca(OH)_2$,[d] % (w/w)	$Ca(OH)_2$,[e] % (v/v)
		(A) EG-*h* + EG-*d*			
0	1.113	1.61	0.265	1.00	0.497
0.099	1.124	1.94	0.882	1.00	0.500
0.194	1.134	2.27	1.48	1.00	0.504
0.294	1.145	2.62	2.13	1.03	0.523
0.497	1.167	3.34	3.47	1.01	0.519
0.600	1.178	3.72	4.18	0.99	0.513
0.796	1.199	4.46	5.55	1.01	0.530
1	1.221	5.26	7.02	1.00	0.531
		(B) 2P-*h* + 2P-*d*			
0	0.786	1.61	0.585	0.91	0.319
0.104	0.796	1.96	1.20	0.94	0.334
0.199	0.806	2.28	1.78	1.00	0.358
0.295	0.816	2.62	2.37	1.02	0.369
0.501	0.837	3.35	3.69	0.99	0.366
0.600	0.848	3.72	4.34	0.99	0.369
0.801	0.869	4.48	5.72	1.05	0.399
1	0.889	5.26	7.15	1.07	0.414
		(C) EG-*h* + 2P-*d*			
0	1.113	1.61	0.265	1.00	0.497
0.101	1.090	1.79	1.07	0.980	0.476
0.199	1.069	1.98	1.82	0.990	0.470
0.314	1.043	2.24	2.68	1.02	0.472
0.496	1.002	2.74	3.95	1.01	0.448
0.603	0.978	3.11	4.67	1.01	0.436
0.794	0.936	3.94	5.89	1.01	0.414
1	0.889	5.26	7.15	1.07	0.413

[a] Solvent weight fraction; χ_{EG-d} in section A and χ_{2P-d} in sections B and C. [b] Particle scattering length density (corrected for hydrogen−deuterium exchange). [c] Solvent scattering length density. [d] Particle weight fraction. [e] Particle volume fraction.

Experimental Section

Ethylene glycol, 2-propanol, sodium hydroxide, and calcium chloride were purchased from Sigma-Aldrich, and deuterated solvents from Eurisotop, France. These were all used as received. Synthesis of the particles was performed as described elsewhere.[19] Samples for neutron scattering were dried, then washed and redispersed in varying proportions of deuterated and nondeuterated solvents. Three sample series were studied, each of varying contrast, consisting of 1% (w/w) nanoparticles dispersed in different solvents: (A) EG (d-6, EG-*d*, and undeuterated); (B) 2P (d-8, 2P-*d*, and undeuterated), and (C) mixtures of EG (undeuterated) and 2P-*d*. The sample compositions and characteristics are outlined in Table 1 below.

SANS studies were performed at the Institut Lange−Langevin, Grenoble, on the D22 small-angle diffractometer. Reduction of SANS data and scaling to absolute scattering intensities was performed on-site by standard procedures; the isotropic two-dimensional data were radially averaged, and the usual corrections for transmission and normalization were made. Measurements were performed in three geometries: two with $\lambda = 6$ Å and sample-to-detector distances (*d*) of 2.0 and 14.4 m, and a third with $\lambda = 16$ Å and $d = 17.6$ m. Due to time constraints, only selected samples were measured in the third, 16 Å/17.6 m geometry, accessing an overall q-range of ~$1.2 \times 10^{-3} < q < 5 \times 10^{-1}$ Å^{-1}. The others were measured only in the first two geometries, accessing a minimum of $q = 5.8 \times 10^{-3}$ Å^{-1}.

SAXS measurements were performed on a Nonius rotating anode (P 4 kW, Cu Kα) with pinhole collimation and a MARCCD detector

(22) Giorgi, R.; Bozzi, C.; Dei, L.; Gabbiani, C.; Ninham, B. W.; Baglioni, P. *Langmuir* **2005**, *21*, 8495.
(23) Giorgi, R.; Chelazzi, D.; Baglioni, P. *Langmuir* **2005**, *21*, 10743.
(24) Baglioni, P.; Carretti, E.; Dei, L.; Giorgi, R. In *Self-Assembly*; Robinson, B. H., Ed.; IOS Press: Amsterdam, 2003.
(25) Baglioni, P.; Giorgi, R. *Soft Matter* **2006**, *2*, 293.
(26) Giorgi, R.; Chelazzi, D.; Carrasco, R.; Colon, M.; Desprat, A.; Baglioni, P. The Maya site of Calakmul: "in situ" preservation of wall paintings and limestone by using nanotechnologies. The Object in Context: Crossing Conservation Boundaries, Munich IIC Congress, The International Institute for Conservation of Historic and Artistic Works, 2006.
(27) Polleux, J.; Pinna, N.; Antonietti, M.; Niederberger, M. *Adv. Mater.* **2004**, *16*, 436.
(28) Spalla, O.; Lyonnard, S.; Testard, F. *J. Appl. Crystallogr.* **2003**, *36*, 338.
(29) Dubois, M.; Gulik-Krzywicki; Cabane, B. *Langmuir* **1993**, *9*, 673.
(30) Ricoul, F.; Dubois, M.; Zemb, T. *J. Phys. II* **1997**, *7*, 69.
(31) Grillo, I.; Levitz, P.; Zemb, T. *Eur. Phys. J. B* **1999**, *10*, 29.
(32) Bartlett, J. R.; Gazeau, D.; Zemb, T.; Woolfrey, J. L. *J. Sol-Gel Sci. Technol.* **1998**, *13*, 113.
(33) Bartlett, J. R. *Prog. Colloid Polym. Sci.* **1997**, *105*, 332.
(34) Bartlett, J. R.; Gazeau, D.; Zemb, T.; Woolfrey, J. L. *Langmuir* **1998**, *14*, 3538.

for data acquisition. The sample-to-detector distance was 105 cm, accessing a minimum q of 0.025 Å^{-1}. Two-dimensional scattering patterns were radially averaged and the intensity was corrected for transmission. Selected samples were also measured by use of a Guinier-Mehring camera with linear collimation and molybdenum anticathode source ($E = 17$ keV, $\lambda = 0.71$ Å), for which the data were scaled to absolute intensity by standard procedures.[35]

Data Treatment. Porod analysis[36] was used to determine the specific particle surface, where at the limit of high q a constant value $A = I(q)q^4$ is obtained according to

$$I(q)q^4 = 2\pi\rho^2\Sigma\varphi_{\text{vol}} \tag{1}$$

with q in reciprocal angstroms, where $I(q)$ is the absolute scattered intensity in reciprocal centimeters, ρ is the contrast per square angstrom, ϕ_{vol} is the particle volume fraction, and Σ is the area of particle surface per unit of particle volume, which for a known particle density can be converted to the specific surface in square meters per gram.

Concentrations were converted to volume fraction by use of literature densities for the solvents and crystalline calcium hydroxide. Densities of mixed solvents were calculated by linear interpolation. In the case of the EG−2P mixtures, the solvent density variation was measured with an Anton Paar DMA-5000 density oscillation tube. Due to the similar densities of 2P-*d* and EG-*h* (0.9 and 1.1, respectively), the difference between the true exponential dependence and linearity was negligible and so is not employed in the following calculations.

Scattering length densities (SLDs) of the solvents and particles were calculated separately for each sample, taking into account the exchange of hydrogen between -OH groups in the particles and the solvent, including the case of the 2P-*d*/EG-*h* mixture where two -OH groups per EG and only one -OD per 2P molecule are exchangeable, changing the weighting of OH:OD in the calcium hydroxide. The contribution of the -OH groups from calcium hydroxide particles ([$Ca(OH)_2$] = 1% by mass) to the overall solvent SLD after exchange was ignored, and the OH:OD ratio in the particles is considered equal to that of the corresponding solvent mixtures. By use of this protocol, the theoretical contrast-match points may also be calculated for each data series.

Treatment of Porod Data. The Porod equation (eq 1) given above can be modified to incorporate a core−shell particle structure, where the single expression for the Porod constant A is split into components for the core and shell:

$$A = I(q)q^4 = 2\pi(\rho^2{}_{\text{c-s}}\phi_{\text{core}}\Sigma_{\text{c-s}} + \rho^2{}_{\text{s-b}}\phi_{\text{shell}}\Sigma_{\text{s-b}}) \tag{2}$$

Here the subscripts c-s and s-b refer respectively to the specific surface areas of the core−shell and shell−bulk interfaces, and concentrations are given as volume fractions. We note that an alternate expression is given by Auvray et al.[37] that includes an oscillating term appearing at high q ($qd > 1$ where d is the distance between the two surfaces):

$$A = 2\pi\Sigma\rho_{\text{c-b}}{}^2(1 + (\rho_{\text{s-c}})(\rho_{\text{s-b}})/\rho_{\text{c-b}}{}^2)(qd^2) \tag{3}$$

They observed this oscillating term by SAXS in ionic surfactant microemulsions where a large electron density accumulates at the surfactant head groups, corresponding to the oil/water interface. Such behavior is best observed in a plot of $I(q)q^4$ versus q^2; however, in the present system no such oscillating term was found, and we therefore use the simple two-interface expression given in eq 2.

Even without knowing the particle morphology, by assuming a thin shell such that $\Sigma = (\Sigma_{\text{c-s}} \sim \Sigma_{\text{s-b}})$, one may reduce eq 2 to

$$A = I(q)q^4 = 2\pi\Sigma(\rho^2{}_{\text{c-s}}\phi_{\text{core}} + \rho^2{}_{\text{s-b}}\phi_{\text{shell}}) \tag{4}$$

Furthermore, if the curvature and roughness of the core−shell interface is small with respect to the shell thickness, the volume fraction of the shell may be related directly to the thickness of the shell:

$$\phi_{\text{shell}} = \phi_{\text{core}}(\Sigma t) \tag{5}$$

This allows the Porod surface to be fitted with only the shell thickness, t, and the shell SLD as fitted parameters. We consider below a core−shell model where the shell is composed also of a solvent mixture, enriched or depleted in one of EG-*h* and 2P-*d*, as a result of adsorption of solvent molecules to the particle surface. Such adsorption is conveniently represented by a Langmuir adsorption isotherm modified for adsorption from binary solution. In this treatment, the amount of a substance adsorbed to a solid surface is given by an exchange constant k, where the difference Q in energy of adsorption between one species and the other is given by[38]

$$k = \text{e}^{-Q/\text{RT}} \tag{6}$$

This exchange constant describes the difference between the amount in the bulk and the fractional surface coverage of one of the species:[38]

$$q/(1 - q) = k[x/(1 - x)] \tag{7}$$

where θ is the surface coverage and x is the bulk composition of that species. Approximating the ideal case, with total surface coverage by the solvent, exchange between the two species on the surface being a 1:1 process, and mixing on the surface being ideal (as in the bulk), this can be rewritten as

$$k = [\phi_{\text{mol,shell}}(1 - \phi_{\text{mol,bulk}})]/[\phi_{\text{mol,bulk}}(1 - \phi_{\text{mol,shell}})] \tag{8}$$

where ϕ_{mol} refers to the mole fraction of one species, in the bulk and in the shell of thickness t, and approximating the surface coverage as the mole fraction in the shell. Reciprocal values k_{2P} and k_{EG} are employed hereafter, referring to the exchange constant with respect to each solvent, where adsorption of the species for which $k > 1$ is favored.

Note also that by using excess concentration rather than surface coverage, there is no specific requirement for monolayer adsorption, and the free energy change refers to a molecule being in a shell of arbitrary thickness t (restricted by the thin-shell assumption defined above), and the SANS data are not directly able to resolve the thickness of such a shell.[39] Nevertheless, it is usually the case in adsorption from condensed media that monolayer adsorption prevails.[38]

SLD_{shell} is then explicitly determined by k, whose value is the sole fitted parameter. For a given t, the shell volume is given by eq 5, and therefore the depletion/enrichment in the bulk solvent, giving SLD_{bulk}, can be calculated to give both the core−shell and shell−bulk contrasts.

An equivalent construction[40] of eq 6 gives k in units of liters per mole. Considering the surface to have an attractive potential of Q joules per mole, that extends a distance of t into the solvent, gives a specific interfacial *volume*, (Σt), in which a specific number of moles of solvent, $(\Sigma t)/V_{\text{mol}}$, is contained, where V_{mol} is the volume of 1 mole of the adsorbing species. In the present construction, the surface is in fact $\Sigma\phi_{\text{vol}}$, the surface area per unit volume of sample, not per unit volume of particle. We then can determine a value of k related to this volume and the depth of the well (energy of adsorption), given by[41]

(35) Né, F.; Grillo, I.; Taché, O.; Zemb, T. *J. Phys. IV* **2000**, *10*, 403.
(36) Porod, G. *Kolloid Z.* **1951**, *124*, 83.
(37) Auvray, L.; Cotton, J. P.; Ober, R.; Taupin, C. *J. Phys.* **1984**, *45*, 913.
(38) Lyklema, J. *Fundamentals of Colloid and Interface Science*; Academic Press: London, 1995; Vol. 2.
(39) Cabane, B.; Zemb, T. *Nature* **1985**, *314*, 385.
(40) Adamson, A. W.; Gast, A. P. *Physical Chemistry of Surfaces*, 6th ed.; Wiley: New York, 1997.
(41) Spalla, O.; Belloni, L. *J. Chem. Phys.* **1991**, *95*, 7689.

$$k^{-1} = (\Sigma\phi_{vol}t)/V_{mol}e^{-Q/RT} \quad (9)$$

Note, however, that in this form k is constant only if the specific surface of the sample is constant.

Results

Figure 1 shows SANS spectra resulting from the contrast-matching determination performed on the two individual solvents. As a preliminary observation, we see that in the case of ethylene glycol, only the q^{-4} Porod limit is observed due to particle agglomeration into micrometer-sized aggregates.[19] In the case of 2-propanol, however, a $\sim(q^{-2.5})$ regime is also observed at low q, indicating a mass-fractal structure[42,43] of the particle aggregates. Selected samples were measured also at double concentration (2% w/w) and then normalized for volume fraction to give identical results.

In the absence of specific adsorption, the contrast match point (CMP) can be determined by a plot of $[I(q)]^{0.5}$ against the solvent SLD at constant q. This plot is linear to either side of the CMP due to the $\Delta\rho^2$ dependence of scattered intensity in the general scattering equation[44,45] and can be verified by determination at several different q values. This does not necessarily give good results in the Porod region due to the combined dependence of the scattered intensity upon both the specific surface and the square of the contrast (eq 1). Nevertheless, if the particle specific surface is known or constant, one should be able to make this determination when the absolute scattered intensity is known. Therefore, the specific surface of the particles in the two solvents, determined from the Porod equation (eq 1), is shown in Figure 2 for each different contrast. The values determined, shown on a log scale for clarity, differ by more than an order of magnitude between the specific surfaces in EG (10^5 cm^{-1}) and 2P (5×10^6 cm^{-1}). It can be seen in both data sets that there is a loss of accuracy, especially on the low-deuterium side, approaching the CMP. In the case of EG, the only precise data are for 100% EG-*h* and EG-*d* samples, as only for these samples was the lowest q range measured. This is also sometimes the case for 2P, but the larger specific surface allowed accurate determination already in the medium q range. The determined values at full contrasts are also given in Table 2The larger surface area in the 2P solvent generally is expected from the results presented in ref 19, where micrometer-sized particle agglomerates are observed in EG, as opposed to the nanosized particles of a few tens of nanometers that were reported in the 2P solvent. This difference was attributed to peptization of the particle surfaces by 2P preventing aggregation into larger agglomerates. Interestingly, an increase by a factor of 1.5 in the specific surface of the particles is observed with increasing deuteration in 2P, suggesting that the deuterated solvent peptizes the surface slightly more effectively. The dashed lines in Figure 2 show the surface determinations by SAXS. Although they are significantly smaller, more importantly the order of magnitude variation between 2P and EG solvents is the same, and the smaller absolute value in the SAXS data is attributed to aging (~1 month) of the particles.

The contrast-matching experiments for the two solvents are presented in Figure 3. Clearly the loss in precision for measurements without the low-q configuration makes the EG samples difficult to interpret.

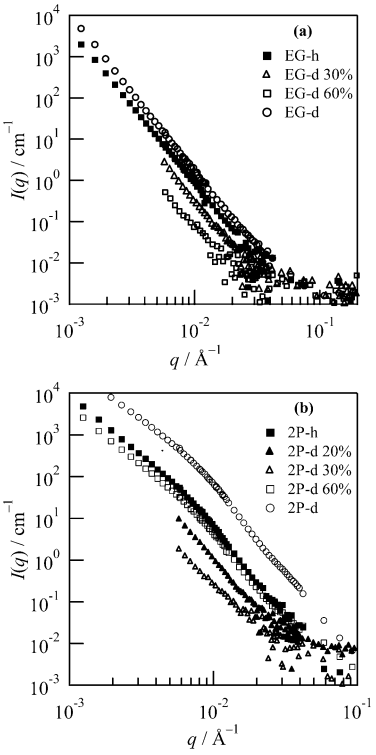

Figure 1. SANS curves at varying contrast from calcium hydroxide nanoparticles dispersed in (a) ethylene glycol and (b) 2-propanol. Proportions of hydrogenated/deuterated solvents are given in weight percent.

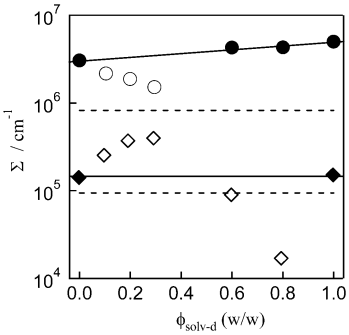

Figure 2. Specific surface areas for $Ca(OH)_2$ nanoparticles in 2P (circles) and EG (diamonds). Open symbols represent samples for which the lowest q-range was not measured, that is, $q_{min} \sim 6 \times 10^{-3}$ Å^{-1}. Data are omitted for the minimum-contrast sample in each case ($SLD_{solv} \sim SLD_{part} \sim 2.5 \times 10^{-6}$ Å^{-2}, occurring near $\phi \sim 0.4$ for both solvents), since the division by the near-zero contrast term results in an unphysical, large exaggeration of the calculated surface. Solid lines are guides to the eye; dashed lines show the respective surface areas as determined by SAXS.

Table 2. Results from Evaluation of the Porod Surfaces in the Four Solvents

solvent	$10^8 \times$ A,[a] cm^{-1}·Å^{-4}	$\Sigma\phi_{vol}$,[b] cm^{-1}	Σ,[c] cm^{-1}	Σ,[c] m^2·g^{-1}
EG-*h*	0.83	733	1.48×10^5	6.6
EG-*d*	1.54	789	1.49×10^5	6.5
2P-*h*	6.38	9.70×10^3	3.04×10^6	135
2P-*d*	48.8	2.20×10^4	5.31×10^6	230

[a] Porod limit. [b] Sample specific surface. [c] Particle specific surface.

The 2-propanol data (Figure 3b), are much clearer. The approach to the calculated CMP is evident and is very precise if the linear variation in the particle surface observed in Figure 2 is employed (solid line). The variation in experimental CMP between the best fit to the data and the interpolated surface is

(42) Hermann, H.; Schmidt, P. W.; Schneider, F. *J. Mater. Sci. Lett.* **1995**, *14*, 816.
(43) Martin, J. E. *J. Appl. Crystallogr.* **1986**, *19*, 25.
(44) Porod, G. In *Small Angle X-Ray Scattering*; Glatter, O., Kratky, O., Eds.; Academic Press: New York, 1982.
(45) Spalla, O. In *Neutrons, X-Rays and Light*; Lindner, P., Zemb, T., Eds.; North-Holland: Amsterdam, 2004.

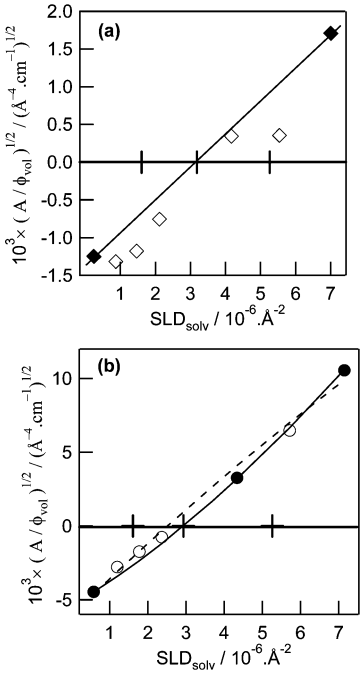

Figure 3. Contrast-matching plots of particles in (a) ethylene glycol and (b) 2-propanol. Calculated zero-contrast points for $Ca(OH)_2$, $Ca(OD)_2$, and fully exchanged particles are indicated on the *x*-axis. The dashed line in panel b is a linear least-squares fit to the presented data, and the solid line is calculated by linearly interpolating the particle surface between the experimentally determined values at $\phi_{2P-d} = 0$ and $\phi_{2P-d} = 1$.

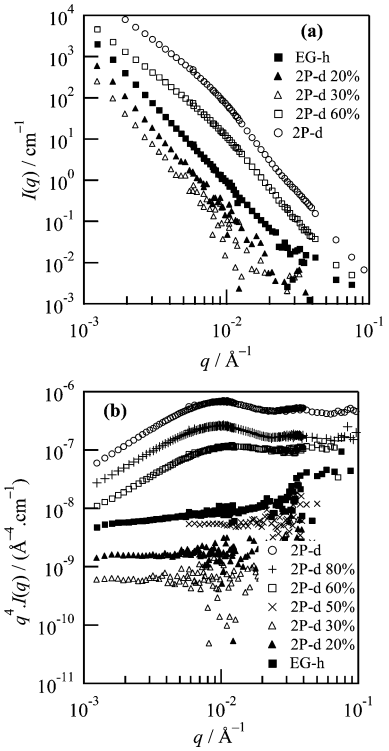

Figure 4. SANS data for 2P-*d*/EG-*h* mixtures: (a) reduced raw data; (b) Porod plot, $q^4I(q)$ vs q. Several data series have been omitted for clarity.

approximately 12%. However, the samples with the least signal-to-noise contribute the greatest variation from the interpolated surface and theoretical CMP.

In order to examine the effect of the solvent on particle aggregation, the SANS spectra of the particles were measured in mixtures of ethylene glycol and deuterated 2-propanol in varying proportions. The raw data in standard log−log and so-called "Porod" representations are shown in Figure 4. Porod law behavior is observed for all samples, as well as oscillation in intensity for the high-signal (deuterated, high-surface) samples that is attributed to surface roughness observable at length scales of $< \sim 50$ nm. The transition from the Porod to fractal regimes that is observed in 2P solvent but not in EG (see Figure 1) is present up to at least 40% EG-*h*, after which there is a transition, between 40% and 70% EG, to the agglomerated particle structure.

The mixture of protonated EG and deuterated 2P requires some care in calculation. As shown in Figure 5a, there is a nonlinear variation of contrast arising from the OH/OD exchange between 2P-*d* (with one -OD group) and EG-*h* (with two -OH groups), and the resulting nonlinear variation in ρ_{part} and $\Delta\rho$ with solvent composition. For the present study, we presume the carbon−hydrogen/deuterium bonds to be nonlabile. Furthermore, we expect a variation in the Porod surface as a function of solvent, thus invalidating a simple CMP extrapolation. Indeed, when examined in the CMP-plot representation, Figure 5b, there is clearly no linearity in the data.

Therefore, it is necessary to determine the particle specific surface independently from the neutron scattering by SAXS. The results are presented in Figure 6. Here the contrast in electronic density is well-known, almost invariable between solvent mixtures, and with no variation due to hydrogen−deuterium exchange. Interestingly, the variation in surface area does not follow a smooth curve, whether linear (as observed between 2P-*h* and -*d*) or logarithmic (as may be expected given

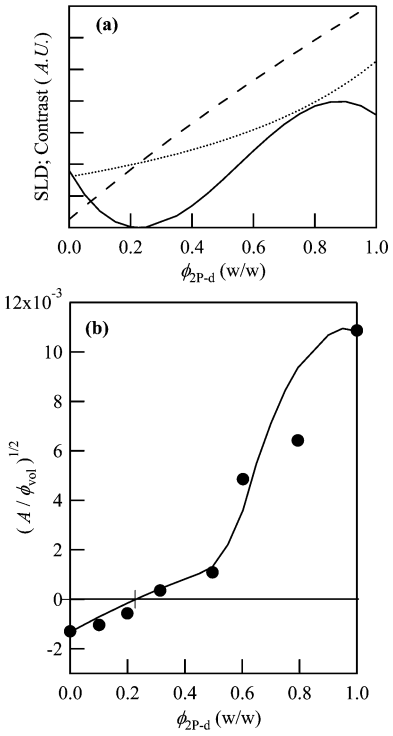

Figure 5. (a) Variation in scattering length densities of the mixed EG-*h*/2P-*d* solvent (− − −), the calcium hydroxide nanoparticles (•••), and the resulting calculated $\Delta\rho^2$ (solid line, $\times 10^6$). (b) Contrast-variation plot of nanoparticles in EG-*h*/2P-*d* solvent mixtures. The line represents the curve calculated from the specific surface of the particles as measured by SAXS (see Figure 6). The calculated CMP for fully deuterium-exchanged particles is indicated on the *x*-axis. The units of *A* are (Å^{-4}·cm^{-1}).

the order of magnitude variation between EG and 2P solvents). Rather, it behaves more like a "titration curve", where only small

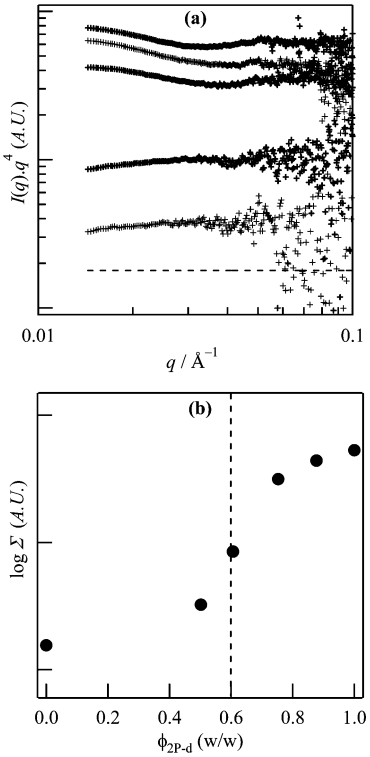

Figure 6. Specific surface as a function of 2P concentration in mixed 2P−EG solvents, as determined by SAXS. (a) Porod plots, $A\,[=q^4I(q)]$ vs q, normalized by volume fraction and contrast, showing the intensity variation in the Porod region. The dashed line indicates the EG surface; the other curves are for ϕ_{2P} (w/w) = 0.5, 0.6, 0.75, 0.9, and 1. (b) Porod specific surface as a function of ϕ_{2P}, showing a titration-shaped surface variation. An approximate "end point" is indicated by the dashed line.

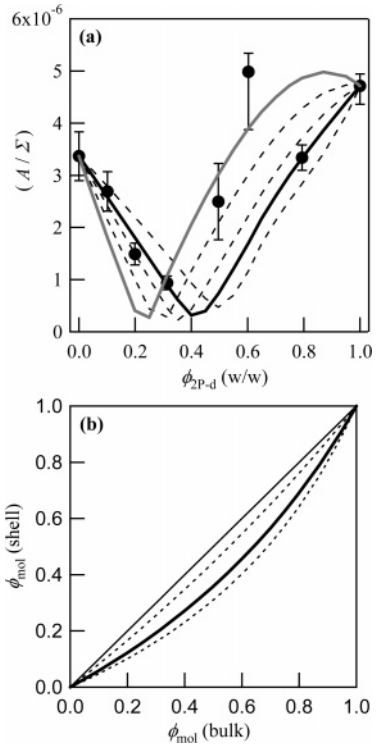

Figure 7. (a) Analysis of the Porod constant A per unit of Σ (as determined by SAXS), normalized by sample volume fractions. Curves are calculated for core−shell structures with surface layer t = 1 nm. The shell composition is determined according to the equilibrium constants k_{2P} (or $k_{EG} = 1/k_{2P}$) = 1 (solid gray line), 0.8, 0.65, 0.56 (best fit, solid black line), and 0.45. (b) Resulting 2P "adsorption isotherms", mole fraction of 2P in the surface layer (shell) as a function of bulk mole fraction, for k_{2P} = 1 (solid line), 0.8, 0.56 (thick solid line), and 0.45.

changes in the surface are observed with solvent composition to either side of an "end point" where there is an abrupt transition between 2P-poor and 2P-rich regions.

When this surface variation is accounted for, a reasonable agreement with the SANS data is obtained (Figure 5b). However, there are still significant discrepancies arising between $\phi_{2P} = 0.6$ and 0.8, as well as in the low-contrast, high-EG-*h* region. The titration-type behavior of the specific surface supports the hypothesis of 2P adsorption being responsible for stabilizing the nanoparticles against agglomeration. If this is the case, the observed behavior suggests a thermodynamic equilibrium between EG and 2P on the surface that drives the transition, and that should be measurable by contrast-variation SANS by use of a more detailed core−shell approach in modeling.

We begin by choosing a shell thickness, t, of 1 nm, or roughly a monolayer of solvent. For several values of k_{EG} and k_{2P}, the contrasts at the two interfaces are calculated as a function of the initial bulk solvent composition, ϕ_{2P}. Rearranging eq 4, we have

$$A/\Sigma = 2\pi(\rho_{c-s}{}^2\phi_{core} + \rho_{s-b}{}^2\phi_{shell}) \qquad (10)$$

Figure 7a shows plots of A/Σ, as a function of overall solvent composition for the SANS data, as well as curves calculated from eq 8 for several values of k_x, normalized to the initial particle volume fraction (which varies between samples with the varying solvent density). For the experimental data points, A is determined from the Porod limit in the SANS data, and Σ is determined by SAXS. Shown in gray is $k_{EG} = k_{2P} = 1$, which maps directly to the curve shown in Figure 4. The negative-to-positive representation of the contrast-matching plot Figure 5b is abandoned in Figure 7, since in a core−shell structure there is no requirement for a total zero-contrast point. Rather the turning point seen at $\rho_{solv} = 2.1 \times 10^{-6}$ Å^{-2} for $k_x = 1$, and increasing for $k_{2P} < 1 < k_{EG}$, represents a "minimum intensity" that is a function of both $\Delta\rho_{c-s}$ and $\Delta\rho_{s-b}$ for a plot of A/Σ. In such a representation, it becomes clear that for a simple surface, the calculated curve does not fit well to the data (Figure 7a, gray curve).

Curves calculated for several values of k_x show the effect of varying the surface layer composition. The data fit well for a constant $k_{2P} = 0.56$ (or $k_{EG} = 1.79$) except at the two points that fall very close, respectively, to the minimum contrast point and the end point in the surface titration. This corresponds to a free energy gain of ∼1.4 kJ·mol^{-1} of EG-*h* over 2P-*d* on the surface, which is in qualitative agreement with calculated relative energies of gas-phase adsorption of EG and 2P onto the bare 001 face of $Ca(OH)_2$.[46] This energy difference is of the order of magnitude of hydrophobic interactions,[47] as might be expected given the formation of a hydrophobic surface when 2P is adsorbed.

Although an apparent constant in units of liters per mole (eq 9) requires a constant specific surface, one can make the calculation in the dilute limit. In this case ethylene glycol has a specific adsorption "constant" (using Σ for the sample in 2P, where EG is dilute) of 4.8 × 10^{-2} M^{-1}, and 2-propanol (using Σ in EG) of 4.1 M^{-1}. Note, however, that these very different values arise only from a difference in the specific surface area, at the same, experimentally determined energy of adsorption, and therefore in the present dynamic, reactive systems do not give useful information. Therefore we consider below only the

(46) Yu, Y. Personal communication.
(47) Tanford, C. *The Hydrophobic Effect: Formation of Micelles and Biological Membranes*, 2nd ed.; Wiley: New York, 1980.

Table 3. Variation of the Best-fit Equilibrium Constants and Corresponding Free Energy of Adsorption[a] at Various Arbitrary Shell Thicknesses

t, nm	0.1	0.5	1	2	2.5
k_{2P}	0.56	0.56	0.56	0.57	0.58
k_{EG}	1.79	1.79	1.79	1.75	1.72
ΔG_{ads}, J·mol^{-1}	−1390	−1390	−1390	−1350	−1300

[a] Free energy of adsorption, ΔG_{ads}, for 2P is equal to $-\Delta G_{ads}$ for EG.

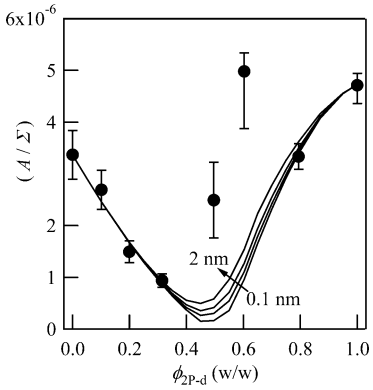

Figure 8. Variation of fitted data as a function of shell thickness, t, for $k_{2P} = 0.56/k_{EG} = 1.79$. $t = 0.1$, 0.5, 1, and 2 nm.

reciprocal, surface-independent values k_{2P} and k_{EG} as defined in eq 8.

Figure 7b shows resulting adsorption isotherms, calculated from eq 8, giving the surface layer composition as a function of total solvent composition, for several values of k_{2P} presented in Figure 7a, including $k_{2P} = 1$ (solid line) and the best-fit value of $k_{2P} = 0.56$ (heavy solid line). Intriguingly, to a first approximation, the end point of the surface titration curve (Figure 6b), occurs at a molar surface coverage of one-half 2P (Figure 7b).

It is likely that an underestimated Σ resulted for the two data points, probably due to a shift in the end point of the surface titration in the samples used for SANS and SAXS. Batch variability or other random error between samples could certainly explain the apparent shift, and the SANS results for the pure 2P solvents (see above) suggest a stronger effect of 2P-*d* on the surface area that would contribute to such a shift. The error bars in Figure 7a partially account for this, due to the larger uncertainty in the SAXS surface determination near the transition point. But even by choosing $\Sigma = \Sigma_{EG}$, curves cannot be fitted to the recalculated data points (see Discussion).

The best-fit values and corresponding ΔG_{ads} are shown in Table 3 for shells of varying thickness, and Figure 8 shows the variation of the fitted curves with the thickness t of the surface layer, at constant k_{2P}. The best-fit curves agree well with the data in the range $t \sim 0.1-2$ nm, consistent with monolayer adsorption ($t \sim 0.6$ nm), which is expected since near-ideal solution behavior is observed for the 2P−EG mixture, and such that neither solvent molecule should be favored in the second layer.

Discussion

The assumption of a thin shell (leading to eq 4) requires that the characteristic distance $\langle \langle H \rangle$, given,[48] by $\langle H \rangle = 3/\Sigma$ for any globular structure of small grains, be greater than the shell thickness t. For the smallest unit particles (in 2P solvent) $\langle H \rangle =$ 5.7 nm, which can be considered an a priori limiting value for t, certainly allowing such an assumption to hold for monolayer adsorption. Note that the value $t = 0$, while not physically meaningful, could also be fitted in principle: Since no consideration of the distance between surfaces (only their contrasts, which are affected by the shell volume and therefore indirectly by the thickness) is included, the two surfaces of different contrast can be arbitrarily close together in the calculation. To the other extreme, for values of $t > \sim 2.5$ nm, the data from the high-surface (2P) samples cannot be fitted to any greater thickness by adjusting k. A similar limiting value can also be found for the low-surface (EG) samples; however, due to the low surface area in the 2P-dilute region, this occurs only at unreasonably large shell thickness.

A general quantitative theory developed by Jolivet et al.[49] for oxide nanoparticle systems showed predictable particle sizes varying as a function of surface energy. Interestingly in the present case, the large specific surface is observed in the less-strongly adsorbing molecule (2-propanol), which would appear to be contrary to the theory of Jolivet (since stronger adsorption should lead to a lower surface energy). However, those particles were studied as a function of pH, thus varying the surface energy through the surface charge density due to protonation and hydroxylation. The solvents in the present case were shown by infrared spectroscopy[19] to be only physisorbed to the surface, and therefore not to affect the surface charge density in the way pH does with oxide nanoparticles. Rather, the specific surface is governed by the hydrophobicity of the surface layer that in the presence of 2-propanol favors smaller particles by slowing down growth on the surface relative to nucleation of separate particles.

For low values of ϕ_{2P} (small Σ), the dependence of the data on t is minimal. This is because t affects only SLD_{bulk} due to enrichment of the shell in one solvent that results in a corresponding depletion in the bulk, which is not significant when the volume fraction of this surface layer (Σt) is infinitesimal with respect to the bulk volume. Therefore the only parameter affected significantly by varying k_{2P} is SLD_{shell}, which then determines both surface contrasts. This is not the case in the high-surface region, where for even quite small t there is significant depletion from the bulk solvent for the fitted shell composition, so that SLD_{bulk} is also dependent upon k.

One may further consider behavior in the intermediate mixtures as nondilute. That is, the assumptions employed here in the Langmuir model of 1:1 exchange and ideal mixing on the surface as well as the bulk are not necessarily valid. Also, the equilibrium shell composition is dependent not only on the energy of adsorption but also on the free energy cost of the concentration gradient (this could also be considered as a shell−bulk surface tension). The rather small ΔG favoring EG over 2P (1.3 kJ·mol^{-1}), being of the order of magnitude of hydrophobic interactions,[47] may then no longer be dominant. Were this the case, one would expect the equilibrium constant to tend toward unity in this region, resulting in the (A/Σ) data that we observe for $\phi_{2P} = 0.5$ and 0.6.

As it is the -OH groups that adsorb to the particles' surface,[19] the number of these groups on each solvent provides a possible simple explanation for the competitive adsorption effect. However, the formation of a hydrophobic interface with the liquid phase by 2P, but not EG, could also contribute. It may be of future interest, therefore, to examine the asymptotic behavior around the transition region more closely in further SANS experiments, to provide further insight into the molecular

(48) Hyde, S.; Anderson, S.; Larsson, K.; Blum, Z.; Landh, T.; Lidin, S.; Ninham, B. W. *The Language of Shape*; Elsevier: Amsterdam, 1997.

(49) Jolivet, J.-P.; Foidefond, C.; Pottier, A.; Chanéac, C.; Cassaignon, S.; Tronc, E.; Euzen, P. *J. Mater. Chem.* **2004**, *14*, 3281.

mechanism of this effect. This may also allow a more detailed model of the adsorption isotherm to be employed than the simple Langmuir case, with the interactions arising in this nondilute region taken into account.[38]

The mass-fractal structure of platelike particle aggregates, observed in samples of $\phi_{2P} > 0.6$, is indicative of diffusion-limited aggregation, with inhibition of the face−face sticking, as a result of adsorbed 2P. Similar phenomena reported recently for mixed metal hydroxides[50] showed low dimensionality ($d \sim 2.3$), from SEM analysis, that results in a "house of cards" structure due to edge−edge and edge−face aggregation. In the present system, there is a continued presence of face−face stacking, resulting in the exaggerated 001 diffraction;[19] however, the specific surface for the 100% 2P sample corresponds to flat particles of thickness ∼8 nm, and the onset of fractal scaling occurs at a length scale of the order ∼70 nm, in close agreement with TEM results,[19] suggesting that individual particles are still resolved, at least in this case. Slightly smaller specific surfaces (i.e., greater apparent thickness), but the same overall range of fractal scaling, is observed for $\phi_{2P} = 0.8$ and 0.6, suggesting an increase in the face−face stacking driven by displacement of 2P by EG, and reaching a critical point at the end point of the "surface titration" that collapses the aggregate structure in the EG regime.

If one analyzes the pure EG-*h* sample more closely, the scaling law at low q ($<\sim 8 \times 10^{-3}$ Å^{-1}) is not quite q^{-4} (Figure 4b). Rather, it is approximately 3.85, characteristic of a slightly fractal surface structure of dimension $d \sim 2.15$.[51] The equivalent scaling is also observed in the EG-*d* sample (not shown). The transition from surface fractal to Porod scaling appears at about the same q as the equivalent transition in the mass fractal of the 2P-rich samples, indicating that the surface fractal is observed on the aggregated superstructure but that the primary particles are unaffected, consistent with the reversibility of the surface area as a function of solvent composition.

Thus the overall effect of adding 2P to such nanoparticle aggregates confirms the proposed[19] hypothesis that adsorption of 2-propanol onto the surface of precipitated calcium hydroxide agglomerates results in a stabilization of the primary nanoparticles. In the case of a mixture of two differently acting solvents, the competition between the two for surface adsorption determines the final aggregate structure (Figure 9a), in this case between open aggregates, where the surface of the subparticles is resolved, and closed aggregates, which appear up to micrometer-sized but are nevertheless separable into nanoparticle units by the addition of appropriate solvent molecules.

It must be noted that one must be skeptical of quantitative fractal dimensions without proper fitting of the data over the full fractal range. This was attempted by use of a structure factor introduced by Teixeira,[52,53] developed for "pearl necklace" structures of spherical subunits on a flexible chain. However, even when the procedure was modified to incorporate a flat particle form factor, good fits could not be found with physically meaningful parameters, and thus this remains a question to be addressed in the future. One exception was found, however, at $\phi_{2P} = 0.6$, close to the end point, where a reasonable overall fit could be found with the apparent size dimension indicated by the onset of fractal scaling, as shown in Figure 9b.

While this simulation remains fairly qualitative, the resultant fractal dimension of ∼1.5, suggests the appearance of many one-dimensional face−face stacks of particles, Figure 9a, as may be expected in the hypothesis presented above for the aggregate structural transition. The lower than expected surface area is the result of constraining the particle dimension to the disc area, rather than thickness, when in fact the individual particles are still mostly resolved in the Porod asymptotic region; however, in any case a quantitative fit could only be expected with consideration of smearing and polydispersity in the model, and this remains a question to be addressed in the future.

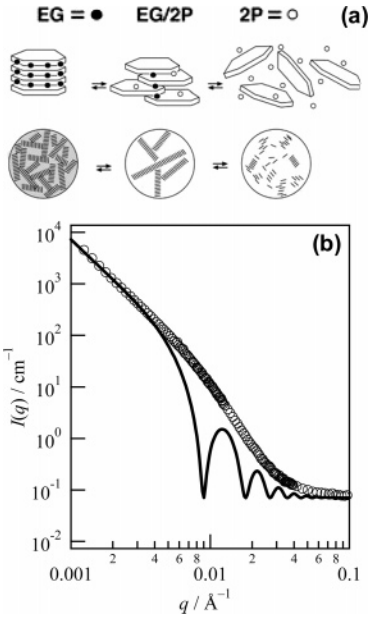

Figure 9. (a) Schematic representation of the structural evolution of aggregates of thin flat discs in varying proportions of the two solvents. In EG, nanocrystals are strongly aggregated such that only micrometer-sized structures are observed by TEM[14] and SANS. In 2P the individual crystals are stabilized by surface adsorption such that individual particles are observed, and in mixtures of the two solvents intermediate structures are observed. The transition is a reversible consequence of thermodynamic, competitive surface adsorption between of the stabilizing 2P and aggregating EG solvents. (b) SANS curve for nanoparticles in 2P-*d* (0.6 w/w) and EG-*h* (data points), and a simulated flat disc form factor and "pearl necklace" structure factor[53] (solid line), using calculated contrast and volume fraction, a disc "thickness" of 70 nm (equal to the approximate particle size), and a fractal dimension of 1.5 (±0.3).

Conclusions

A process resulting from simple adsorption of solvent molecules onto particle surfaces, in an otherwise additive-free system, has significant implications with respect to aggregation and growth phenomena and could help to account for, for example, mechanisms of inorganic crystal growth under the influence of adsorbent polymeric additives that stabilize precursor particles. Calcium carbonate especially can assemble in a variety of ways to form the final crystal structures, including oriented attachment and formation of so-called mesocrystals, which have been observed to display a mass-fractal distribution of adsorbing polymer[54,55] and have been claimed to be mesoporous in structure and specific surface area.[9,56,57] We have shown that competitive adsorption with just a small favorability in energy on the order

(50) Jin, Z. L.; Hou, W. G.; Li, X. W.; Sun, D. J.; Zhang, C. G. *Chin. Chem. Lett.* **2005**, *16*, 835.
(51) Teixeira, J. *J. Appl. Crystallogr.* **1988**, *21*, 781.
(52) Chen, S.-H.; Teixeira, J. *Phys. Rev. Lett.* **1986**, *57*, 2583.
(53) Liu, Y. C.; Sheu, E. Y.; Chen, S.-H.; Storm, D. A. *Fuel* **1995**, *74*, 1352.
(54) Endo, H.; Schwahn, D.; Cölfen, H. *J. Chem. Phys.* **2004**, *120*, 9410.
(55) Endo, H.; Schwahn, D.; Cölfen, H. *Physica B* **2004**, *350*, e943−e945.
(56) Wang, T.; Antonietti, M.; Cölfen, H. *J. Am. Chem. Soc.* **2005**, *127*, 3246.
(57) Wohlrab, S.; Pinna, N.; Antonietti, M.; Cölfen, H. *Chem.*−Eur. J. **2005**, *11*, 2903.

of magnitude of hydrophobic interactions provides an effective, highly sensitive means to reversibly modify nanoparticle aggregation by a simple but structure-directing small molecule such as 2-propanol, resulting in an ordered assembly. This provides further insight into the "second step" of additive-controlled crystallization, where nucleated precursor particles, that can be stabilized in nanocrystalline, amorphous, or microgel-like moieties, can undergo assembly into coherent larger scale structures.

Acknowledgment. We kindly acknowledge Dr. B.Salvadori for her help with preparation and purification of $Ca(OH)_2$ nanoparticles, and the Institut Laue—Langevin for provision of beamtime on D22. M.G.P. acknowledges the DFG, CNRS, and CEA for financial support within the German—French Network. E.F., R.G., and P.B. acknowledge CSGI (Florence, Italy) and MIUR for partial financial support.

LA062023I